ChemPubSoc Europe

DOI: 10.1002/chem.201403751

CHEMISTRY
A European Journal
Communication

Single-Molecule Magnets

Large Spin-Relaxation Barriers for the Low-Symmetry Organolanthanide Complexes [Cp*$_2$Ln(BPh$_4$)] (Cp* = pentamethylcyclopentadienyl; Ln = Tb, Dy)

Selvan Demir, Joseph M. Zadrozny, and Jeffrey R. Long*[a]

Abstract: Single-molecule magnets comprising one spin center represent a fundamental size limit for spin-based information storage. Such an application hinges upon the realization of molecules possessing substantial barriers to spin inversion. Axially symmetric complexes of lanthanides hold the most promise for this due to their inherently high magnetic anisotropies and low tunneling probabilities. Herein, we demonstrate that strikingly large spin reversal barriers of 216 and 331 cm^{-1} can also be realized in low-symmetry lanthanide tetraphenylborate complexes of the type [Cp*$_2$Ln(BPh$_4$)] (Cp* = pentamethylcyclopentadienyl; Ln = Tb (**1**) and Dy (**2**)). The dysprosium congener showed hysteretic magnetization data up to 5.3 K. Further studies of the magnetic relaxation processes of **1** and **2** under applied dc fields and upon dilution within a matrix of [Cp*$_2$Y(BPh$_4$)] revealed considerable suppression of the tunneling pathway, emphasizing the strong influence of dipolar interactions on the low-temperature magnetization dynamics in these systems.

Molecules showing slow magnetic relaxation and magnetic hysteresis as a result of an energy barrier to spin inversion, known as single-molecule magnets, could ultimately serve as the smallest conceivable unit for spin-based devices. Indeed, their ability to maintain spin orientation for a long time at low temperatures makes them attractive candidates for potential applications in spintronics devices and high-density information storage.[1–2] However, such possible applications require molecules with large energy barriers to spin reversal to stabilize data integrity against thermal fluctuations. This requirement is met in highly symmetric mononuclear transition-metal[3–5] and lanthanide[6–14] complexes that possess large axial magnetic anisotropies or strongly coupled systems that contain radical ligands bridging between magnetically anisotropic metal ions,[15–18] in which tunneling processes, which undercut the energy barrier with respect to reorientation, are suppressed. The magnetic moments of lanthanide complexes are particularly prone to large barriers, because they can possess a tremendous single-ion anisotropy arising from unquenched orbital angular momentum and strong spin–orbit coupling. Naturally, the records for single-molecule magnet figures of merit such as spin reversal barrier (U_{eff})[11] and blocking temperature (T_B)[17] are held by lanthanide-based species.

Recently, it has been shown that radical-bridging ligands, such as N_2^{3-} or bipyrimidine$^{\cdot-}$ (bpym$^{\cdot-}$), engender strong magnetic-exchange coupling in dilanthanide species, despite the contracted 4f electron density.[16–18] The observation of large U_{eff} values despite the low molecular symmetry of these species makes one wonder if the single-ion anisotropies are somehow assisted by the exchange coupling to generate a large overall magnetic anisotropy. Several studies have explored the nature of the exchange interaction and its impact on U_{eff} in the N_2^{3-} radical-bridged complexes, and recent results suggest that the observed barrier is indeed linked more strongly to the magnitude of the exchange coupling than to the molecular magnetic anisotropy.[19–20] Studies of the magnetic anisotropies of mononuclear fragments of the radical-bridged species are thus essential to resolve the contribution of anisotropy to U_{eff} in the presence of the exchange. In the course of conducting such studies, we discovered large relaxation barriers in low-symmetry organolanthanide complexes of the type [Cp*$_2$Ln(BPh$_4$)] (Cp* = pentamethylcyclopentadienyl; Figure 1). These results pose a remarkable finding, because high symmetry is generally viewed as requisite for generating such large barriers.[15]

Lanthanide complexes of the type [Cp*$_2$Ln(BPh$_4$)] have been utilized for a variety of applications, including, for example, the activation of small molecules.[21–22] The syntheses of [Cp*$_2$Tb(BPh$_4$)] (**1**) and [Cp*$_2$Dy(BPh$_4$)] (**2**) proceed readily through the reaction of [Cp*$_2$Ln(C$_3$H$_5$)] with HNEt$_3$BPh$_4$.[18] X-ray diffraction studies of single crystals of **1** and **2** revealed that they are isostructural, with the metal center and boron atom residing on a twofold rotation axis in the crystal (Figure 1).[18] The lanthanide ion is coordinated in the usual bent manner by two Cp* ligands, but only very weakly by the tetraphenylborate ion through agostic interactions involving two of the phenyl rings, a situation also found in the La, Nd, Sm, and Y congeners.[23–25] A unique feature of these molecules is that the metal ion experiences a ligand field that is neither axial nor strongly equatorial in nature.

[a] Dr. S. Demir, Dr. J. M. Zadrozny, Prof. Dr. J. R. Long
Department of Chemistry
University of California Berkeley (USA)
Berkeley, CA 94720-146
Fax: (+1) 510-643-3546
E-mail: jrlong@berkeley.edu

Supporting information for this article is available on the WWW under http://dx.doi.org/10.1002/chem.201403751.

© 2014 Wiley-VCH Verlag GmbH & Co. KGaA, Weinheim

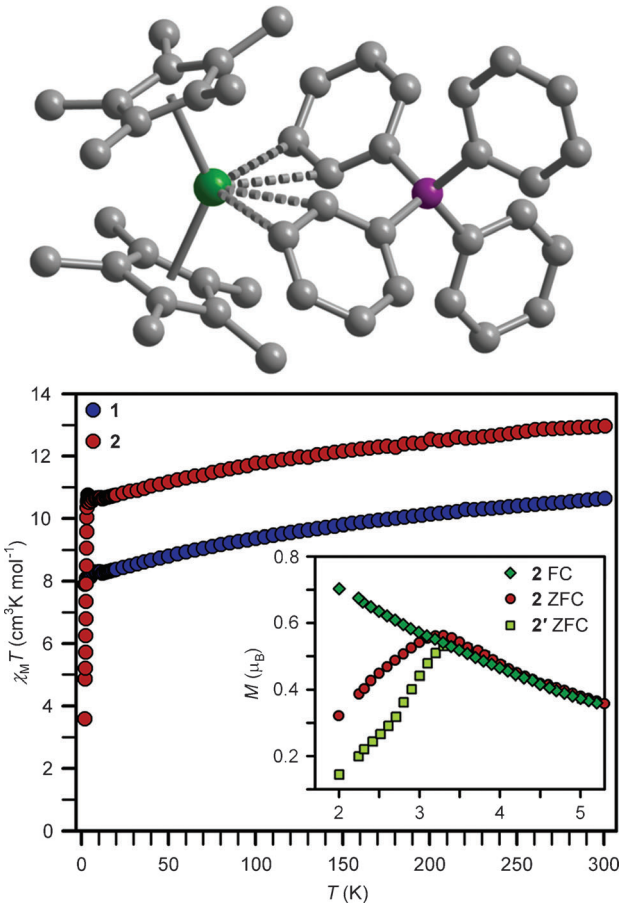

Figure 1. Top: structure of the $[Cp^*_2Dy(BPh_4)]$ complex in a crystal of **2**, exhibiting a point group symmetry of C_2. Green, purple, and gray spheres represent Dy, B, and C atoms, respectively; hydrogen atoms are omitted for clarity. Compound **1** is isostructural. Bottom: variable-temperature dc magnetic susceptibility data for restrained polycrystalline samples of **1** and **2** collected under a 1 kOe applied dc field. Inset: plot of magnetization versus temperature during field-cooled (green squares) and zero-field-cooled (red circles) measurements for **2** and for **2′** (1:4(1) Dy/Y dilution) showing the thermoremnant magnetization.

Variable-temperature dc magnetic susceptibility data collected for **1** and **2** revealed the presence of significant magnetic anisotropy (Figure 1). The room-temperature $\chi_M T$ values of 10.64 and 12.96 cm^{3}K mol^{-1} for **1** and **2**, respectively, are slightly lower than the expected values of 11.81 and 14.17 cm^{3}K mol^{-1} for the corresponding free Ln^{3+} ions. With decreasing temperature, a slight decrease in $\chi_M T$ occurs for **1**, reaching a minimum of 7.89 cm^{3}K mol^{-1} at 2 K. Similarly, $\chi_M T$ gradually decreases for **2** when the temperature is lowered, but sharply plummets at 3.4 K. Such a sharp decrease in $\chi_M T$ for molecular systems can be a strong indication of magnetic blocking. Indeed, zero-field cooled and field-cooled magnetic-susceptibility data collected for **2** revealed a sharp divergence of the two data sets at 3.2 K (inset of Figure 1), confirming a strong pinning of the magnetic moments below that temperature.

The magnetization relaxation dynamics of compounds **1** and **2** were investigated through variable-temperature, variable-frequency ac magnetic-susceptibility measurements. Both compounds showed in-phase (χ_M') and out-of-phase (χ_M'') ac susceptibility signals indicative of long magnetic relaxation times (Figures 2, S2, and S3 in the Supporting Information). At 2 K and zero dc field, **1** exhibited a peak maximum at 1000 Hz that decreased in intensity with increasing temperature (Figure S1 in the Supporting Information). Under these same conditions, **2** instead revealed a fully resolved peak at 10.4 Hz, which decreased in intensity first with rising temperature before moving to higher frequencies starting at 12 K. Applied dc fields ranging from 200 to 2400 Oe strongly influenced the shape of the χ_M'' frequency scan for both **1** and **2** (Figures 2, S4 and S5 in the Supporting Information). With increasing dc field, a decline in the intensities of the higher frequency peaks occurred for both complexes in concert with the appearance of peaks at lower frequency. With further increasing field, the high-frequency peaks were completely eliminated. The change in the low-frequency peak with increasing field appeared to saturate for **1** and **2** at 2400 and 1600 Oe, respectively (Figures S4 and S5 in the Supporting Information). Variable-temperature ac susceptibility measurements of **1** and **2** at these dc fields revealed much stronger temperature dependences than were observed at zero-applied dc field (Figures 2, S6, and S7 in the Supporting Information).

The influence of dipole-mediated magnetic interactions on the ac susceptibility data for **1** and **2** was evaluated through analyses of the isostructural compounds $[Cp^*_2Tb_{0.33}Y_{0.67}(BPh_4)]$ (**1′**) and $[Cp^*_2Dy_{0.25}Y_{0.75}(BPh_4)]$ (**2′**). Herein, the paramagnetic Tb^{III} and Dy^{III} complexes are effectively diluted in a matrix of diamagnetic $[Cp^*_2Y(BPh_4)]$,[25] in which **1′** corresponds to a 1:3 Tb/Y dilution, and **2′** to a 1:4 Dy/Y dilution. For both compounds **1′** and **2′**, the observed peaks at zero-applied dc field displayed significantly more prominent temperature-dependent regimes than the respective pure samples (Figures S8 and S10 in the Supporting Information). However, regimes in which the peak maxima are temperature independent are still apparent for these species at the lowest temperatures of the measurement, though at lower frequencies. Overall, this behavior suggests that magnetization relaxation through quantum tunneling is substantially, but not entirely, suppressed upon dilution of the complexes to these levels. Notably, the temperature-independent regimes in **1′** and **2′** are effectively extinguished under 2400 and 1600 Oe dc fields, respectively, as was also observed for the pure complexes (Figures S9 and S11 in the Supporting Information).

Derivation of the temperature dependence of the magnetic relaxation times (τ) allowed quantitation of the magnitude of U_{eff}, as well as visualization of the various pathways through which the magnetic moments can invert. Determination of this information first proceeded by extraction of τ from the fits of Cole–Cole plots for all species to a generalized Debye function (Figures S12–S18 in the Supporting Information). The resulting data were then used to construct Arrhenius plots, as presented in Figure 3. The Orbach process of spin reversal proceeds through thermal excitation over a potential-energy barrier and imparts an exponential dependence of τ upon temperature through the relationship $\tau = \tau_0 \exp(U_{eff}/k_B T)$, in which τ_0 is the attempt time and k_B is the Boltzmann constant. This tempera-

© 2014 Wiley-VCH Verlag GmbH & Co. KGaA, Weinheim

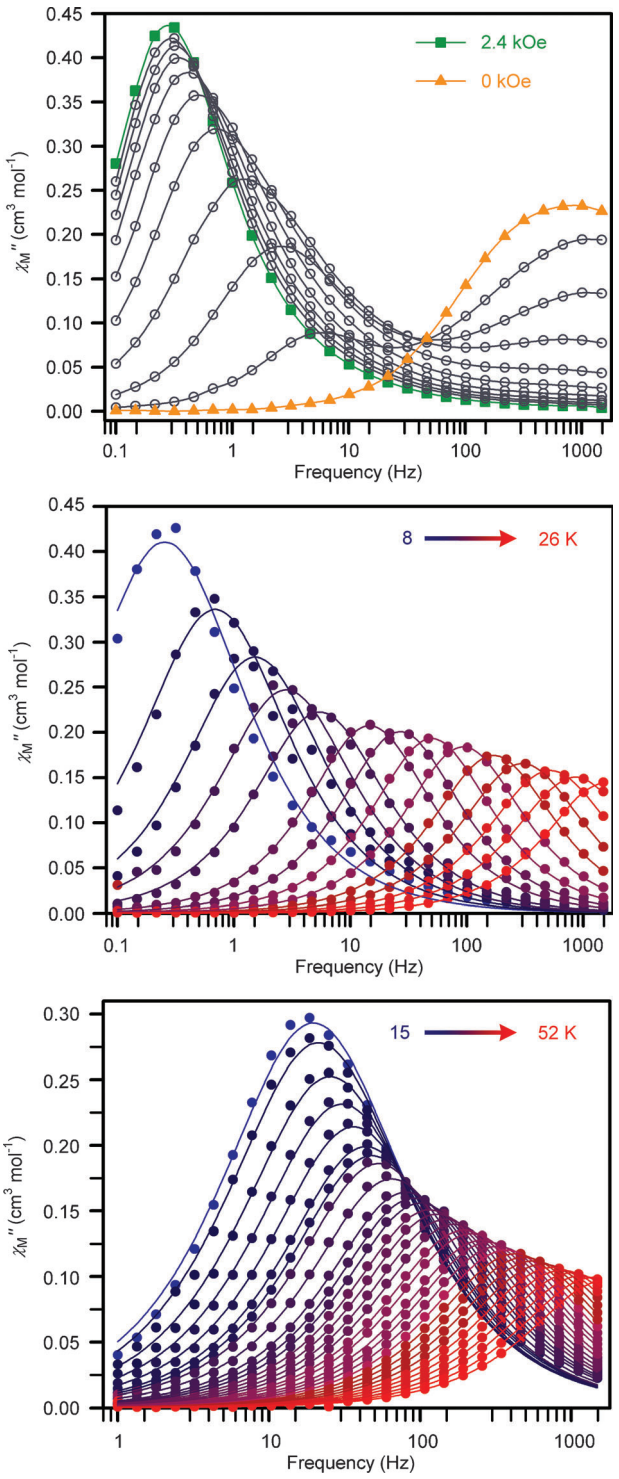

Figure 2. Top: out-of-phase ac susceptibility (χ_M'') collected on pure **1** at 8 K under dc fields ranging from 0 Oe to 2.4 kOe in 200 Oe increments, in which the 2000 and 2200 Oe data set were eliminated for clarity. Solid lines are guides for the eye. Middle: out-of-phase ac magnetic susceptibility for **1** under 2400 dc field from 8 K (blue circles) to 26 K (red circles). Solid lines represent fits to the data. Bottom: out-of-phase (χ_M'') component of the ac magnetic susceptibility for **2** under zero-applied dc field, shown from 15 K (blue circles) to 52 K (red circles). Solid lines represent fits to the data, as was described in the main text.

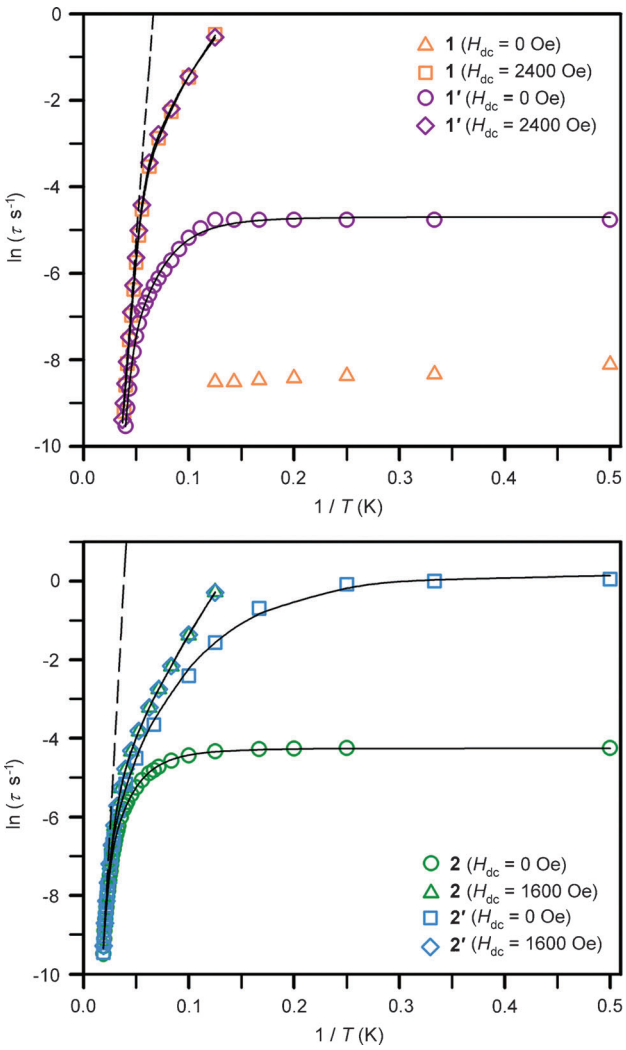

Figure 3. Arrhenius plots of relaxation time data for **1** and **1**′ (top), and **2** and **2**′ (bottom). Solid black lines correspond to fits to multiple relaxation processes, as was described in the main text of the report and the Supporting Information. The best fits for **1** and **1**′ (H_{dc} = 2400 Oe), and **2** and **2**′ (H_{dc} = 1600 Oe) yield values of U_{eff} of 221, 216, 314, and 331 cm^{-1}, respectively, and values of τ_0 of 5×10^{-10}, 8.0×10^{-10}, 2×10^{-8}, and 1×10^{-9} s, respectively. The dashed black lines represent the best fits to the data for **1**′ and **2**′ between 20 and 27 K and 45 and 52 K, respectively, with $\tau_0 = 5\times10^{-10}$ s and U_{eff} = 216 cm^{-1} (top) and $\tau_0 = 1\times10^{-9}$ s and U_{eff} = 331 cm^{-1} (bottom).

ture dependence should give a linear slope in the Arrhenius plots of Figure 3, but in actuality, the plots are substantially curved. This curvature indicates that the moments of **1** and **2** have access to multiple pathways for spin reversal, which impart varying temperature dependences to τ. Thus, the plots shown in Figure 3 were fit to multiple relaxation processes, enabling accurate determination of the relaxation barriers (see Figure 3 and the Supporting Information for details). These fits required Orbach, Raman, and quantum-tunneling processes[26] to model the data for **1**, **1**′, **2**, and **2**′ successfully (see also Figures S19 and S20 in the Supporting Information). The obtained values of τ_0 and U_{eff} are comparable between the pure and dilute samples for **1** and **2**; however those obtained for **1**′ and **2**′ under applied dc fields are expected to be more accurate due to the extended linear regimes. In complexes **1**′ and **2**′, these values are 216 and 331 cm^{-1} for U_{eff} and 8×10^{-10} and

© 2014 Wiley-VCH Verlag GmbH & Co. KGaA, Weinheim

1×10^{-9} s for τ_0, respectively. The values of U_{eff} are surprisingly large, whereas those of τ_0 are within the expected range for single-molecule magnets.[2]

The relaxation barriers of **1** and **2** are of the highest known for single-molecule magnets. Of the terbium single-molecule magnets reported to date, only the family of well-studied phthalocyanine sandwich complexes possess higher barriers, with the record corresponding to $U_{eff}=652$ cm^{-1}.[11] Additionally, the barrier in **2** is the largest observed to date for a mononuclear dysprosium complex. Of the known dysprosium-based single-molecule magnets, only the multinuclear dysprosium alkoxide clusters exhibit higher barriers for which doping dysprosium into a Y_4K_2 cluster matrix gave $U_{eff}=585$ cm^{-1}.[27–28] Typical barriers for dysprosium-based single-molecule magnets are much less than 100 cm^{-1}.[29] The exceptions to this are $[Dy(paaH)_2(H_2O)_4Cl_3\cdot 2H_2O]$, $[Dy(dpq)(acac)]_3$, $[(sal)(MeOH)Dy(NO_3)(\mu\text{-}L)ZnBr]$ (in which paaH = *N*-(2-pyridyl)-ketoacetamide ;dpq = dipyridoquinoxaline; Hsal = salicylaldehyde; L = a Schiff-base ligand), and $[Zn_2Dy(L')_2(MeOH)](NO_3)\cdot 3MeOH\cdot H_2O$, which exhibited barriers of 124, 130, 234, and 305 cm^{-1}, respectively.[30–36]

Importantly, the high relaxation barriers for the aforementioned species are generally attributed to a uniaxial ligand field. This is a result of the oblate electron distributions associated with the maximal $\pm M_J$ levels of the spin–orbit coupled ground states of Tb^{III} and Dy^{III}.[15] Consistent with such a model, variation of the ligands of the Zn_2Dy complex revealed a stark drop in U_{eff} with a decrease in the axiality of the coordination sphere of the Dy^{III} center.[35] Thus, complexes **1** and **2** are remarkable in that they lack a clear axis of symmetry in the ligand field but nevertheless possess U_{eff} values that are among the highest reported for single-molecule magnets. Notably, $[Cp^*_2Dy(BPh_4)]$ exhibited the highest relaxation barrier yet observed for a metallocene compound, even higher than COT^{2-}-based (COT^{2-} = cyclooctatetraene dianion) organoerbium(III) single-molecule magnets that are reasoned to show slow magnetic relaxation based on their equatorial ligand field.[9,12–13] Indeed, this species displays the highest barrier reported to date for any organometallic complex, assuming the strict definition that the molecule must contain at least one metal–carbon bond.

Variable-field magnetization measurements were performed on **1** and **2** to check for magnetic hysteresis in light of the large observed spin reversal barriers. For compound **1**, a very slight hysteresis arises for nonzero values of *H* at 1.8 K (Figure S21 in the Supporting Information). In comparison, hysteresis loops observed for **2** are significantly more pronounced (Figure 4) and remain open with increasing temperature until 5.3 K, although the loops all close suddenly at zero applied field, leaving no remanent magnetization. The apparent slowing of the relaxation time upon dilution observed on the ac timescale extended into the time domain of the dc measurements. For example, the open regions of the hysteresis loops are slightly enhanced in the diluted species **1**′ and **2**′ (Figures S21 and S22 in the Supporting Information). It is further worth noting that the $\chi_M T$ plot of **2**′ showed a more pronounced blocking at 2 K than that of **2**, with $\chi_M T$ dropping to

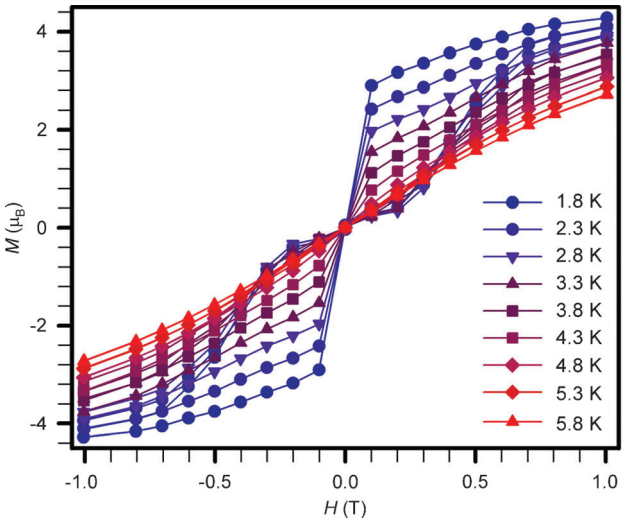

Figure 4. Variable-field magnetization (*M*) data for compound **2** collected from 1.8 to 5.8 K at an average sweep rate of 0.002 Ts^{-1}.

a minimum value of 1.63 versus 3.58 cm^3 K mol^{-1}, respectively (inset of Figure 1 and Figure S23 in the Supporting Information). Nevertheless, fast magnetic-relaxation processes at zero field persisted despite the dilution, suggesting either that dipolar interactions are still prompting tunneling at the dilution levels of **1a** and **2a** or that other fast relaxation mechanisms are present.

On the basis of these observations, we attribute the lack of a remanent magnetization for **1** and **2** to the coexistence of tunneling pathways and a dipole-mediated magnetic avalanche.[12] Such an explanation agrees well with the low-temperature ac susceptibility data, in which fast-relaxation pathways are considerably slowed by application of a modest dc field or dilution in a diamagnetic matrix. A major facilitator of tunneling is asymmetry in the ligand field, which can introduce transverse anisotropies that mix the levels of the ground $\pm M_J$ doublet.[37] Notably, Kramers ions, such as Dy^{III}, do not undergo such a level mixing,[38] and this difference between **1** and **2** may explain the discrepancy in the magnetic relaxation times observed at zero field and low temperature, and further why blocking and open hysteresis were observed for **2**, but not for **1**. Another important indicator of a reduced tunneling influence for **2** is apparent in the lower dc field required to match the effect of the dilution. Dipolar effects scale with moment magnitude and distance, the latter remaining constant across **1** and **2**, whereas the $\chi_M T$ data revealed the moment to be larger for **2**. Thus, the Tb^{III} complex in **1** would be expected to experience weaker dipolar effects that would require less of a dc field magnitude to mitigate. Observation of the opposite trend, in which a stronger field is required to shut down the dipolar effects in **1**, likely confirms the prevalence of other fast relaxation pathways in **1** over **2**.

The program Magellan was used to extract information about the magnetic easy axis in **2** in view of the apparently asymmetric ligand field.[39] As was revealed by the computation, the axis of preferred alignment extends between the

© 2014 Wiley-VCH Verlag GmbH & Co. KGaA, Weinheim

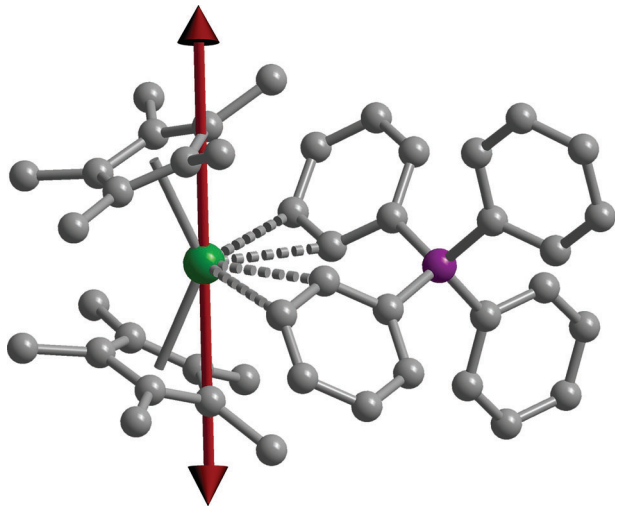

Figure 5. Orientation of the main anisotropy axis in **2**. Coordinates are taken from the crystal structure depicted in Figure 1. The same general orientation of the easy axis is obtained for the other molecule within the asymmetric unit of the crystal structure.

most separated carbon atoms of the two Cp* rings (Figure 5). This alignment is akin to that obtained by ab initio methods for the dinuclear species $[\{Cp'_2Dy(\mu\text{-}SSiPh_3)\}_2]$ ($Cp' = \eta^5\text{-}C_5H_4Me$), which features similar coordination geometries about the Dy^{III} ion and a ground $M_J = \pm {}^{15}/_2$ doublet.[40] Note that Dy^{III} and Tb^{III} centers share the same general aspherical electron density, such that the results for **2** should also extend to **1**.

The large barriers displayed by **1** and **2** are unexpected due to the visually nonaxial ligand field of the complexes. Typically, low-symmetry elements of a ligand field are invoked as facilitators of tunneling or other magnetic-relaxation processes that undermine the observation of true thermally activated relaxation. On the basis of the Magellan output, we found that a very weak ligand, the BPh_4^- anion, interacts with the lanthanide ions in the hard plane, where the biggest contribution to tunneling would be expected. Thus, we speculate that such large U_{eff} values arise directly from the bent ligand field presented to the Ln^{III} centers within the $[Cp^*_2Ln(BPh_4)]$ complexes. Herein, the weak agostic interactions between the metal centers and the phenyl rings of the BPh_4^- anion make a negligible contribution to the ligand field. The weak ligand fields imposed on the Ln^{III} ions by the BPh_4^- anions in **1** and **2** can therefore be viewed not as engendering a large overall magnetic anisotropy, but rather leading to a weak transverse anisotropy. A comparison between the magnetization dynamics of **2** and $[\{Cp'_2Dy(\mu\text{-}SSiPh_3)\}_2]$ supports this interpretation, because the much stronger $SSiPh_3^-$ ligands can be expected to generate greater transverse components to the magnetic anisotropy. Indeed, because transverse anisotropy can lead to enhancements in the prevalence of non-Orbach relaxation pathways, we also noted that the Arrhenius plots for **1** and **2** are noticeably simpler than that for $[\{Cp'_2Dy(\mu\text{-}SSiPh_3)\}_2]$, which appears highly curved over the entire temperature range of investigation. Although tunneling is likely enhanced by a stronger ligand field in the hard plane, an alternative (or additional) possibility is that a strong ligand field in the hard plane serves to strongly mix the M_J levels and lower their total splitting. These separate ligand-field effects are likely responsible for the lower observed barrier in the dinuclear species relative to **2**. We acknowledge that the dinuclear nature of $[\{Cp'_2Dy(\mu\text{-}SSiPh_3)\}_2]$ likely complicates the comparison with **2**, because dipolar effects are expected to be highly active in the former species.

Interestingly, the barriers obtained for **1** and **2** are much larger than those found for the bipyrimidyl radical-bridged complexes $[(Cp^*_2Ln)_2(\mu\text{-}bpym^{\cdot})]^+$ (Ln = Tb ($U_{eff} = 44\ cm^{-1}$), Dy ($U_{eff} = 88\ cm^{-1}$)), which incorporate similar bent $[Cp^*_2Ln]^+$ moieties.[18] A recent report of a radical-bridged dinuclear transition-metal complex revealed that magnetic relaxation at low temperature occurred through a single excitation to the lowest-lying exchange-coupled M_S level,[41] rather than multiple excitations, which is common for higher-nuclearity systems.[2] Thus, the larger barriers in **1** and **2** relative to the dinuclear species may imply that the spin reversal barrier in the dilanthanide species is governed more by the strength of the magnetic coupling than by the contributions from the single-ion magnetic anisotropy. If this is true, then the Orbach relaxation likely proceeds via the lowest-lying exchange-coupled state, rather than through the first-excited M_J level of the ground-state moment (see Figure S24 in the Supporting Information). In addition, or even alternatively, the anisotropy may be largely quenched by the stronger ligand-field contribution of the $bpym^{\cdot-}$ ligand compared to the weakly coordinating BPh_4^- anion. It is possible that the anisotropy may also be further diluted by the increased spin of the dinuclear complex relative to the mononuclear fragments.[42]

The foregoing results demonstrate that the bent ligand fields presented within the complexes $[Cp^*_2Ln(BPh_4)]$ (Ln = Tb, Dy) generated single-molecule magnets with unusually high magnetic anisotropy barriers. Future efforts will include an investigation of the effects of replacing BPh_4^- with various other weakly coordinating anions on the relaxation dynamics.

Acknowledgements

This work was funded by NSF Grant No. CHE-1010002. We thank the Postdoctoral Program of the German Academic Exchange Service (DAAD) for fellowship support of S.D., and M. I. Gonzalez for experimental assistance.

Keywords: lanthanides · magnetic anisotropy · magnetic properties · single-molecule magnets

[1] M. N. Leuenberger, D. Loss, *Nature* **2001**, *410*, 789.
[2] D. Gatteschi, R. Sessoli, J. Villain, *Molecular Nanomagnets*, Oxford University Press, Oxford, **2006**.
[3] Y.-Y. Zhu, C. Cui, Y.-Q. Zhang, J.-H. Jia, X. Guo, C. Gao, K. Qian, S.-D. Jiang, B.-W. Wang, Z.-M. Wang, S. Gao, *Chem. Sci.* **2013**, *4*, 1802.
[4] J. M. Zadrozny, D. J. Xiao, M. Atanasov, G. J. Long, F. Grandjean, F. Neese, J. R. Long, *Nat. Chem.* **2013**, *5*, 577.
[5] J. M. Zadrozny, M. Atanasov, A. M. Bryan, C.-Y. Lin, B. D. Rekken, P. P. Power, F. Neese, J. R. Long, *Chem. Sci.* **2013**, *4*, 125.

© 2014 Wiley-VCH Verlag GmbH & Co. KGaA, Weinheim

[6] N. Ishikawa, M. Sugita, T. Ishikawa, S.-y. Koshihara, Y. Kaizu, *J. Am. Chem. Soc.* **2003**, *125*, 8694.
[7] M. A. AlDamen, J. M. Clemente-Juan, E. Coronado, C. Martí-Gastaldo, A. Gaita-Ariño, *J. Am. Chem. Soc.* **2008**, *130*, 8874.
[8] K. Katoh, T. Kajiwara, M. Nakano, Y. Nakazawa, W. Wernsdorfer, N. Ishikawa, B. K. Breedlove, M. Yamashita, *Chem. Eur. J.* **2011**, *17*, 117.
[9] S.-D. Jiang, B.-W. Wang, H.-L. Sun, Z.-M. Wang, S. Gao, *J. Am. Chem. Soc.* **2011**, *133*, 4730.
[10] M. Jeletic, P.-H. Lin, J. J. Le Roy, I. Korobkov, S. I. Gorelsky, M. Murugesu, *J. Am. Chem. Soc.* **2011**, *133*, 19286.
[11] C. R. Ganivet, B. Ballesteros, G. de La Torre, J. M. Clemente-Juan, E. Coronado, T. Torres, *Chem. Eur. J.* **2013**, *19*, 1457.
[12] K. R. Meihaus, J. R. Long, *J. Am. Chem. Soc.* **2013**, *135*, 17952.
[13] L. Ungur, J. J. Le Roy, I. Korobkov, M. Murugesu, L. F. Chibotaru, *Angew. Chem.* **2014**, *126*, 4502; *Angew. Chem. Int. Ed.* **2014**, *53*, 4413.
[14] P. Zhang, L. Zhang, C. Wang, S. Xue, S.-Y. Lin, J. Tang, *J. Am. Chem. Soc.* **2014**, *136*, 4484.
[15] J. D. Rinehart, J. R. Long, *Chem. Sci.* **2011**, *2*, 2078.
[16] J. D. Rinehart, M. Fang, W. J. Evans, J. R. Long, *Nat. Chem.* **2011**, *3*, 538.
[17] J. D. Rinehart, M. Fang, W. J. Evans, J. R. Long, *J. Am. Chem. Soc.* **2011**, *133*, 14236.
[18] S. Demir, J. M. Zadrozny, M. Nippe, J. R. Long, *J. Am. Chem. Soc.* **2012**, *134*, 18546.
[19] T. Rajeshkumar, G. Rajaraman, *Chem. Commun.* **2012**, *48*, 7856.
[20] Y.-Q. Zhang, C.-L. Luo, B.-W. Wang, S. Gao, *J. Phys. Chem. A* **2013**, *117*, 10873.
[21] W. J. Evans, D. S. Lee, C. Lie, J. W. Ziller, *Angew. Chem.* **2004**, *116*, 5633; *Angew. Chem. Int. Ed.* **2004**, *43*, 5517.
[22] B. M. Schmiege, J. W. Ziller, W. J. Evans, *Inorg. Chem.* **2010**, *49*, 10506.
[23] W. J. Evans, C. A. Seibel, J. W. Ziller, *J. Am. Chem. Soc.* **1998**, *120*, 6745.
[24] H. Hamaed, A. Y. H. Lo, D. S. Lee, W. J. Evans, R. W. Schurko, *J. Am. Chem. Soc.* **2006**, *128*, 12638.
[25] W. J. Evans, B. L. Davis, T. M. Champagne, J. W. Ziller, *Proc. Natl. Acad. Sci. USA* **2006**, *103*, 12678.
[26] L. J. Berliner, S. S. Eaton, G. R. Eaton in *Biological Magnetic Resonance, Vol. 19* (Eds.: L. J. Berliner, S. S. Eaton, G. R. Eaton), Kluwer Academic/Plenum Publishers, New York, **2000**.
[27] R. J. Blagg, C. A. Muryn, E. J. L. McInnes, F. Tuna, R. E. P. Winpenny, *Angew. Chem.* **2011**, *123*, 6660; *Angew. Chem. Int. Ed.* **2011**, *50*, 6530.
[28] R. J. Blagg, L. Ungur, F. Tuna, J. Speak, P. Comar, D. Collison, W. Wernsdorfer, E. J. L. McInnes, L. F. Chibotaru, R. E. P. Winpenny, *Nat. Chem.* **2013**, *5*, 673.
[29] D. N. Woodruff, R. E. P. Winpenny, R. A. Layfield, *Chem. Rev.* **2013**, *113*, 5110.
[30] A. Watanabe, A. Yamashita, M. Nakano, T. Yamamura, T. Kajiwara, *Chem. Eur. J.* **2011**, *17*, 7428.
[31] H_2L = 6,6′-(1E,1′E)-(2,2-dimethylpropane-1,3-diyl)bis(azan-1-yl-1-ylidene)-bis(methan-1-yl-1-ylidene)bis(2-methoxyphenol) and symbolizes the Schiff-base ligand.
[32] G.-J. Chen, Y.-N. Guo, J.-L. Tian, J. Tang, W. Gu, X. Liu, S.-P. Yan, P. Cheng, D.-Z. Liao, *Chem. Eur. J.* **2012**, *18*, 2484.
[33] N. F. Chilton, S. K. Langley, B. Moubaraki, A. Soncini, S. R. Batten, K. S. Murray, *Chem. Sci.* **2013**, *4*, 1719.
[34] paaH = N-(2-pyridyl)-ketoacetaminde, dpq = dipyridoquinoxaline.
[35] J.-L. Liu, Y.-C. Chen, Y.-Z. Zheng, W.-Q. Lin, L. Ungur, W. Wernsdorfer, L. F. Chibotaru, M.-L. Tong, *Chem. Sci.* **2013**, *4*, 3310.
[36] L′ = 2,2′,2′′-(((nitrilotris(ethane-2,1-diyl))tris(azanediyl))tris(methylene))tris-(4-bromophenol).
[37] D. Gatteschi, R. Sessoli, *Angew. Chem.* **2003**, *115*, 278; *Angew. Chem. Int. Ed.* **2003**, *42*, 268.
[38] H. A. Kramers, *Proc. R. Acad. Sci. Amsterdam* **1930**, *33*, 959.
[39] N. F. Chilton, D. Collison, E. J. L. McInnes, R. E. P. Winpenny, A. Soncini, *Nat. Commun.* **2013**, *4*, 2551.
[40] F. Tuna, C. A. Smith, M. Bodensteiner, L. Ungur, L. F. Chibotaru, E. J. L. McInnes, R. E. P. Winpenny, D. Collison, R. A. Layfield, *Angew. Chem.* **2012**, *124*, 7082; *Angew. Chem. Int. Ed.* **2012**, *51*, 6976.
[41] I.-R. Jeon, J. G. Park, D. J. Xiao, T. D. Harris, *J. Am. Chem. Soc.* **2013**, *135*, 16845.
[42] F. Neese, D. A. Pantazis, *Faraday Discuss.* **2011**, *148*, 229.

Received: May 30, 2014
Published online on June 26, 2014

© 2014 Wiley-VCH Verlag GmbH & Co. KGaA, Weinheim